

***4f* and *5d* levels of Ce^{3+} in D_2 eightfold oxygen coordination**

Luis Seijo^{1,2,*} and Zoila Barandiarán^{1,2}

¹*Departamento de Química, Universidad Autónoma de Madrid, 28049 Madrid, Spain*

²*Instituto Universitario de Ciencia de Materiales Nicolás Cabrera,
Universidad Autónoma de Madrid, 28049 Madrid, Spain*

(Dated: June 21, 2018)

Abstract

The effects on the *4f* and *5d* levels of Ce^{3+} of its first coordination shell geometry in Ce-doped oxides with a D_2 8-fold site, like garnets, are studied with embedded cluster, wave function based *ab initio* methods. The only deformations of a CeO_8 cube that are found to shift the lowest *4f* \rightarrow *5d* transition to the red are the symmetric Ce-O bond compression and the tetragonal symmetric bond bending. These results are analyzed in terms of centroid and ligand field stabilization energy differences. The splittings of the upper *5d* levels and of the *4f* levels are also discussed.

Keywords: Cerium, Ce^{3+} , *4f*, *5d*, D_2 , oxides, garnets, 8-fold coordination

I. INTRODUCTION

Yttrium aluminum garnet $\text{Y}_3\text{Al}_5\text{O}_{12}$ (YAG) doped with Ce^{3+} is a well known phosphor with a blue $\text{Ce}^{3+} 4f \rightarrow 5d$ absorption and a corresponding yellow $5d \rightarrow 4f$ emission,¹ which is used in InGaN blue LED based, white light solid-state lighting devices.^{2,3} In the search for alternative phosphors with the best efficiencies and tailored color-rendering indexes, doping Ce^{3+} in other artificial garnets has been a line of work. It led, for instance, to the discoveries of the $\text{Lu}_2\text{CaMg}_2\text{Si}_3\text{O}_{12}:\text{Ce}^{3+}$ orange phosphor⁴ and the $\text{Ca}_3\text{Sc}_2\text{Si}_3\text{O}_{12}:\text{Ce}^{3+}$ green phosphor.⁵

Most garnets can be described in terms of a 160 atom body-centered cubic unit cell (80 atom primitive cell) of the $Ia\bar{3}d$ (230) space group, which contains eight formula units of $\text{A}_3\text{B}'_2\text{B}''_3\text{O}_{12}$. A, B' and B'' are cations of different nominal charges in different symmetry sites. In $\text{Y}_3\text{Al}_5\text{O}_{12}$, for instance, $\text{A}\equiv\text{Y}$, $\text{B}'\equiv\text{Al}$, and $\text{B}''\equiv\text{Al}$,⁶ all with oxidation states +3. In $\text{Ca}_3\text{Sc}_2\text{Si}_3\text{O}_{12}$, $\text{A}\equiv\text{Ca}$, $\text{B}'\equiv\text{Sc}$, and $\text{B}''\equiv\text{Si}$,⁷ with respective oxidation states +2, +3, and +4. In $\text{Lu}_2\text{CaMg}_2\text{Si}_3\text{O}_{12}$, 2/3 of the A sites are occupied by Lu and 1/3 by Ca atoms,⁴ and $\text{B}'\equiv\text{Mg}$, and $\text{B}''\equiv\text{Si}$, with respective oxidation states +3, +2, +2 and +4. In all cases, A occupy 24(c) sites of 8-fold coordination, B' 16(a) sites of 6-fold coordination, and B'' 24(d) sites of 4-fold coordination, all of them at fixed positions, with the remaining 96 O atoms in (h) sites, which depend on three x , y and z internal parameters.⁶ Optically active Ce^{3+} impurities substitute for A atoms at (c) sites, which have the local symmetry of the D_2 point group and a first coordination shell made of 8 oxygen atoms.

The energies of the $4f$ and $5d$ levels of Ce^{3+} in particular garnets and in other oxides depend on the bonding and electrostatic interactions between Ce and the hosts, and they can be calculated in a one-by-one basis, with reasonable accuracy, by means of *ab initio* methods, both in D_2 local symmetry like in Ce-doped YAG⁸ and in lower local symmetries like in Ce,La-doped YAG⁹ and Ce,Ga-doped YAG.¹⁰ These energies are dominated, up to first-order, by the bonding interactions between Ce and its first oxygen coordination shell, subject to the basic confinement embedding effects of the host. Other specific host embedding effects are important at higher orders of approximation and they refine the results.

This paper is aimed at providing a basic study of the energies of the levels of the $4f^1$ and $5d^1$ manifolds of Ce^{3+} in D_2 8-fold oxygen coordination. We report the results of an *ab initio* calculation of them after consideration of the bonding interactions with the first

oxygen coordination shell only, under the effects of a cubic, non host specific, confinement embedding potential. The present results are a common reference for these levels of Ce^{3+} in specific garnets (and other oxides with 8-fold coordination), since the latter can be considered as resulting from the former after including the host specific embedding effects.

II. METHOD

In order to know the $4f^1$ and $5d^1$ energy levels of Ce^{3+} under the effects of its interactions with a coordination shell of eight oxygens in a D_2 symmetry site of a solid oxide, we calculated the corresponding energy levels of the $(\text{CeO}_8)^{13-}$ cluster embedded in a O_h host potential. We will describe later the details of the *ab initio* wave function based quantum mechanical calculation. With the choice of a cubic host embedding potential, all the energy splittings and changes due to D_2 distortions are ascribable to the interactions between Ce and the first-shell O atoms.

It is convenient to look at the D_2 energy levels as derived from the more familiar O_h levels after geometry distortions and this is what we did in this work. In consequence with this, we decided to take a cubic CeO_8 O_h moiety as a reference and to choose six atomic displacement coordinates $S_1 - S_6$ that transform according to irreducible representations of the O_h point symmetry group for the six degrees of freedom of the CeO_8 D_2 moiety. They are defined in Table I and represented in Fig. 1. S_1 represents the breathing (or symmetric bond stretching) of the reference cube and it transforms according to the totally symmetric irreducible representation a_{1g} ; S_2 represents an asymmetric bond stretching of the crosses $a_1 - a_2 - a_3 - a_4$ and $e_1 - e_3 - e_2 - e_4$ and it transforms according to the $e_g\epsilon$ sub-species of the doubly degenerate e_g irreducible representation;¹¹ S_3 and S_4 are the $e_g\theta$ and $e_g\epsilon$ symmetric and asymmetric bond bendings of the a and e crosses; and S_5 and S_6 are the $e_u\theta$ and $e_u\epsilon$ symmetric and asymmetric twistings of the crosses.

The details of the quantum mechanical calculation are the following. We performed *ab initio* calculations on a $(\text{CeO}_8)^{13-}$ cluster that include Ce-O bonding effects, static and dynamic electron correlation effects, scalar and spin-orbit coupling relativistic effects, and cubic host embedding effects. For each D_2 nuclear configuration of the $(\text{CeO}_8)^{13-}$ embedded cluster, we performed, in a first step, scalar relativistic calculations with the many-electron second-order Douglas-Kroll-Hess (DKH) Hamiltonian.^{12,13} These were state-

average complete-active-space self-consistent-field^{14–16} (SA-CASSCF) calculations with the active space that results from distributing the open-shell electron in 13 active molecular orbitals with main character Ce $4f$, $5d$, $6s$, which provided occupied and empty molecular orbitals to feed subsequent multi-state second-order perturbation theory calculations (MS-CASPT2),^{17–20} where the dynamic correlation of 73 electrons (the $5s$, $5p$, $4f$, $5d$, $6s$ electrons of Ce and $2s$, $2p$ electrons of the O atoms) were taken into account. In a second step, spin-orbit coupling effects were included by adding the AMFI approximation of the DKH spin-orbit coupling operator²¹ to the Hamiltonian and performing restricted-active-space state-interaction spin-orbit calculations (RASSI-SO)²² with the previously computed SA-CASSCF wave functions and MS-CASPT2 energies.

In all these calculations, the Hamiltonian of the $(\text{CeO}_8)^{13-}$ cluster is supplemented with a cubic embedding Hamiltonian. For this we chose the *ab initio* model potential embedding Hamiltonian (AIMP)²³ of a SrO host with CsCl lattice structure ($Pm\bar{3}m$, no. 221), which provides a perfect 8-fold cubic oxide coordination of the cationic site. We used a lattice constant $a = 2.87 \text{ \AA}$ (the one that gives a Ce-O equilibrium distance in the cubic $(\text{CeO}_8)^{13-}$ embedded cluster of 2.34 \AA at the MS-CASPT2 level of calculation, which is the Ce-O distance of the reference CeO_8 cube in an hypothetical undistorted Ce-doped YAG⁶). The embedding potential of this 8-fold coordinated cubic oxide was computed in Hartree-Fock self-consistent embedded-ions calculations (SCEI),²⁴ in which the input embedding AIMPs used for the Sr^{2+} and O^{2-} ions of SrO are consistent with the output AIMPs obtained out of the HF orbitals of the embedded Sr^{2+} and O^{2-} ions.

III. RESULTS

The dependence of the $4f \rightarrow 4f$ and $4f \rightarrow 5d$ transitions on the D_2 distortions of the first coordination shell are shown in Fig. 2 without spin-orbit coupling and in Fig. 3 with spin-orbit coupling interactions included. The chosen ranges of the $S_1 - S_6$ coordinates span their usual values in natural and artificial garnets, which are shown in Table II and in the figures. Besides the transitions, the figures include two additional lines: One is the difference between the $5d$ and $4f$ energy centroids (or average energies of the five $5d^1$ levels and the seven $4f^1$ levels), $\Delta E_{centroid,fd} = E_{centroid}(5d^1) - E_{centroid}(4f^1)$; the other is the difference between the ligand field stabilization energies of the $5d$ and $4f$ lowest levels $\Delta E_{ligand\ field,df} =$

$[E_{centroid}(5d^1) - E_1(5d^1)] - [E_{centroid}(4f^1) - E_1(4f^1)]$. The fact that the lowest $4f \rightarrow 5d$ transition equals their subtraction, $E_1(5d^1) - E_1(4f^1) = \Delta E_{centroid,fd} - \Delta E_{ligand\ field,df}$, has been used to analyze the reasons behind red and blue shifts of this transition.^{9,10}

Let us first focus on the lowest $4f \rightarrow 5d$ transition, whose reverse is the luminescence of Ce^{3+} in garnets and other oxides. It is clear that only two coordinates have an important impact on it: the breathing mode S_1 , which does not distort the cubic symmetry, and the symmetric bond bending mode S_3 , which gives a $e_g\theta$ tetragonal distortion of the CeO_8 cube.

Symmetric compression of the Ce-O bonds lowers the $4f \rightarrow 5d$ transition. This is almost entirely due to the increase of the $5d$ ligand field it produces, which lowers the first $5d^1$ level with respect to its centroid. This effect is slightly compensated with a small increase due to the centroids: bond compression slightly shifts the $5d$ centroid upwards with respect to the $4f$ centroid. The latter observation has been made before^{10,25} and it contradicts the predictions of the usual model for the centroid energy difference,²⁶⁻²⁸ according to which it should be smaller for smaller bond lengths; nevertheless, the model has been useful to rationalize $5d \rightarrow 4f$ luminescences.²⁹ The contribution of the breathing mode S_1 to the lowest $4f \rightarrow 5d$ transition represented in Fig. 3 fits $8255 S_1 - 4803 S_1^2$; for cubic CeO_8 moieties $S_1 = 2\sqrt{2}\Delta d$, Δd being the Ce-O bond length change with respect to the reference cube; in our case the reference cube has Ce-O bond length of 2.34 Å and a lowest $4f \rightarrow 5d$ transition of 26000 cm^{-1} .

Symmetric bond bending along the S_3 coordinate lowers the $4f \rightarrow 5d$ transition. Among the D_2 distortions of the cube, it is the only tetragonal one. Also, it is the only one with a significant impact on the transition (for the ranges of $S_2 - S_6$ shown by garnets). The enhancement of tetragonal distortions of the cube as responsible for the red-shifts of the Ce^{3+} luminescence has been suggested by Cheetham and coworkers³⁰ and it is supported by the present investigation. The image emerging from an analysis in terms of configurational energy centroids and ligand field stabilization is one in which the lowering of the first $5d^1$ level with respect to the ground state is due in almost equal amounts to an increase of the ligand field (of its tetragonal component) and to a reduction of the centroid energy difference. Again, the latter effect contradicts the prediction of the Judd-Morrison model: a very small increase of the centroid energy difference out of a very small increase of the Ce-O distances. The contribution of the tetragonal mode S_3 to the lowest $4f \rightarrow 5d$ transition represented in Fig. 3 fits $1844 S_3 - 2885 S_3^2$ for $S_3 < 0$ and $-1876 S_3 - 141 S_3^2$ for $S_3 > 0$.

This contribution is due in almost equal amounts to the lowering of the centroid energy difference and the increasing of the ligand field. The centroid effect fits $10 S_3 - 2695 S_3^2$ for $S_3 < 0$ and $12 S_3 - 2581 S_3^2$ for $S_3 > 0$; the ligand field effect fits $1834 S_3 - 190 S_3^2$ for $S_3 < 0$ and $-1887 S_3 + 2440 S_3^2$ for $S_3 > 0$.

Apart from S_1 and S_3 , only the asymmetric stretching S_2 has an effect, although very small, on the first $4f \rightarrow 5d$ transition (it fits $-2033 S_2^2$ in the range of the figures).

Regarding higher $4f \rightarrow 5d$ transitions, several remarks can be made from Figs. 2 and 3. The gap between the first and the second $5d$ levels related with the cubic 2E_g is due to the symmetric bending S_3 and to the symmetric twisting S_5 , with a significantly higher contribution from the latter in garnets; however, different splittings in different garnets would be due to S_3 . The splitting of the three upper levels, mostly related with the cubic ${}^2T_{2g}$, comes basically from the symmetric bending S_3 and the asymmetric stretching S_2 , with a small contribution from the symmetric twisting S_5 and negligible contributions from the asymmetric bending and twisting S_4 and S_6 . The larger S_1 and the absolute values of S_2 and S_3 , the higher probability for the third $5d$ level to appear below the conduction band of the garnet.

Finally, the $4f$ levels are shown with more detail in Figs. 4 and 5, without and with spin-orbit coupling respectively. These may be interesting because the $5d \rightarrow 4f$ emission is made of the superposition of the seven individual emissions and the full width and shape of the emission band depends, although not only, on the relative positions of the $4f$ levels. Since the emission to the highest $4f$ level has a minor contribution to the full emission band shape,⁸ we can have a predictive hint by looking at the six lowest $4f$ levels. According to Fig. 5, the width seems to be controlled by S_2 and S_3 , so that the garnets with higher absolute values of these two coordinates would tend to have wider emission bands because of their higher $4f$ level separation. Of course, the width of each individual $5d \rightarrow 4f$ emission will depend on the $5d$ and $4f$ equilibrium offsets.

IV. CONCLUSIONS

The levels of the $4f^1$ and $5d^1$ manifolds of Ce^{3+} in D_2 8-fold oxygen coordination have been calculated *ab initio* as a function of D_2 deformation coordinates of a reference cube, with the goal of pinpointing the effects of the geometry of the first coordination shell. A

(CeO₈)¹³⁻ cluster under the effects of a confinement AIMP embedding potential of cubic symmetry has been used at a level of calculation all-electron DKH for the Hamiltonian and SA-CASSCF/MS-CASTP2/RASSI-SO for the wave functions. The results include bonding, correlation, scalar relativistic, spin-orbit coupling, and embedding interactions.

It is found that the lowest $4f \rightarrow 5d$ transition shifts significantly to the red only as a consequence of symmetric Ce-O bond compression and tetragonal symmetric bond bending.

The increase of the $5d$ cubic ligand field dominates the effects of the bond compression, whereas the effect of the tetragonal bond bending distortion is divided in almost equal amounts between an increase of the $5d$ tetragonal ligand field and a reduction of the energy difference between the $5d$ and $4f$ energy centroids.

The splittings of the upper $5d$ levels and of the $4f$ levels have also been studied.

Acknowledgments

This work was partly supported by a grant from Ministerio de Economía y Competitividad, Spain (Dirección General de Investigación y Gestión del Plan Nacional de I+D+I, MAT2011-24586).

* Corresponding author; Electronic address: luis.seijo@uam.es

¹ G. Blasse and A. Brill, *J. Chem. Phys.* **47**, 5139 (1967).

² S. Nakamura and G. Fasol, *The blue laser diode: GaN based light emitters and lasers* (Springer, Berlin, 1997).

³ T. Jüstel, H. Nikol, and C. Ronda, *Angew. Chem., Int. Ed.* **37**, 3084 (1998).

⁴ A. A. Setlur, W. J. Heward, Y. Gao, A. M. Srivastava, R. G. Chandran, and M. V. Shankar, *Chem. Mater.* **18**, 3314 (2006).

⁵ Y. Shimomura, T. Honma, M. Shigeiwa, T. Akai, K. Okamoto, and N. Kijima, *J. Electrochem. Soc.* **154**, J35 (2007).

⁶ F. Euler and J. A. Bruce, *Acta Crystallogr.* **19**, 971 (1965).

⁷ S. Quartieri, R. Oberti, M. Boiocchi, M. C. Dalconi, F. Boscherini, O. Safonova, and A. B. Woodland, *Am. Mineral.* **91**, 1240 (2006).

- ⁸ J. Gracia, L. Seijo, Z. Barandiarán, D. Curulla, H. Niemansverdriet, and W. van Gennip, *J. Lumin.* **128**, 1248 (2008).
- ⁹ A. B. Muñoz-García, J. L. Pascual, Z. Barandiarán, and L. Seijo, *Phys. Rev. B* **82**, 064114 (2010).
- ¹⁰ A. B. Muñoz-García and L. Seijo, *Phys. Rev. B* **82**, 184118 (2010).
- ¹¹ S. Sugano, Y. Tanabe, and H. Kamimura, *Multiplets of Transition-Metal Ions in Crystal* (Academic, New York, 1970).
- ¹² M. Douglas and N. M. Kroll, *Ann. Phys. (N.Y.)* **82**, 89 (1974).
- ¹³ B. A. Hess, *Phys. Rev. A* **33**, 3742 (1986).
- ¹⁴ B. O. Roos, P. R. Taylor, and P. E. M. Siegbahn, *Chem. Phys.* **48**, 157 (1980).
- ¹⁵ P. E. M. Siegbahn, A. Heiberg, B. O. Roos, and B. Levy, *Phys. Scr.* **21**, 323 (1980).
- ¹⁶ P. E. M. Siegbahn, A. Heiberg, J. Almlöf, and B. O. Roos, *J. Chem. Phys.* **74**, 2384 (1981).
- ¹⁷ K. Andersson, P.-Å. Malmqvist, B. O. Roos, A. J. Sadlej, and K. Wolinski, *J. Phys. Chem.* **94**, 5483 (1990).
- ¹⁸ K. Andersson, P.-Å. Malmqvist and B. O. Roos, *J. Chem. Phys.* **96**, 1218 (1992).
- ¹⁹ A. Zaitsevskii and J. P. Malrieu, *Chem. Phys. Lett.* **233**, 597 (1995).
- ²⁰ J. Finley, P.-Å. Malmqvist, B. O. Roos and L. Serrano-Andrés, *Chem. Phys. Lett.* **288**, 299 (1998).
- ²¹ B. A. Hess, C. M. Marian, U. Wahlgren, and O. Gropen, *Chem. Phys. Lett.* **251**, 365 (1996).
- ²² P. A. Malmqvist, B. O. Roos, and B. Schimmelpfennig, *Chem. Phys. Lett.* **357**, 230 (2002).
- ²³ Z. Barandiarán and L. Seijo, *J. Chem. Phys.* **89**, 5739 (1988).
- ²⁴ L. Seijo and Z. Barandiarán, *J. Chem. Phys.* **94**, 8158 (1991).
- ²⁵ Z. Barandiarán, N. M. Edelstein, B. Ordejón, F. Ruipérez, and L. Seijo, *J. Solid State Chem.* **178**, 464 (2005).
- ²⁶ B. R. Judd, *Phys. Rev. Lett.* **39**, 242 (1977).
- ²⁷ C. A. Morrison, *J. Chem. Phys.* **72**, 1001 (1980).
- ²⁸ M. Bettinelli and R. Moncorgé, *J. Lumin.* **92**, 287 (2001).
- ²⁹ P. Dorenbos, *J. Lumin.* **87-89**, 970 (2000).
- ³⁰ J. L. Wu, G. Gundiah, and A. K. Cheetman, *Chem. Phys. Lett.* **441**, 250 (2007).
- ³¹ J. Ganguly, W. Cheng, and H. S. C. O'Neill, *Am. Mineral.* **78**, 583 (1993).
- ³² T. Armbruster, C. A. Geiger, and G. A. Lager, *Am. Mineral.* **77**, 512 (1992).

- ³³ C. A. Geiger and T. Armbruster, *Am. Mineral.* **82**, 740 (1997).
- ³⁴ B. Etschmann, V. Streltsov, N. Ishizawa, and E. N. Maslen, *Acta Crystallogr. B* **57**, 136 (2001).
- ³⁵ A. Nakatsuka, A. Yoshiasa, and S. Takeno, *Acta Crystallogr. B* **51**, 737 (1995).
- ³⁶ G. Patzke, R. Wartchow, and M. Binnewies, *Z. Kristallogr.* **214**, 143 (1999).
- ³⁷ H. Sawada, *J. Solid State Chem.* **132**, 300 (1997).

TABLE I: Definitions of the D_2 totally symmetric displacements of the CeO_8 moiety chosen in this work: Stretching, bending, and twisting O_h symmetry coordinates. The labels of the oxygen atoms and the chosen cartesian axes are defined in Fig. 1: In the reference cube, the symmetry independent oxygen atoms a_1 and e_1 are located at $(\sqrt{2}, 0, 1)d/\sqrt{3}$ and $(0, \sqrt{2}, 1)d/\sqrt{3}$ respectively, with d being the Ce-O distance. \hat{R} is the D_2 symmetrization operator: the normalized addition of the group symmetry operations (the identity and the three 180° rotations around the cartesian axes). δx_{a1} is the x cartesian displacement of the Oxygen atom $a1$ from its position in the reference cube: $\delta x_{a1} = x_{a1} - x_{a1,ref}$; identical definitions stand for the other cartesian displacements.

$\hat{R} = \frac{1}{2} (\hat{I} + \hat{C}_{2x} + \hat{C}_{2y} + \hat{C}_{2z})$		
Displacement	O_h irrep	Definition
symmetric stretching	a_{1g}	$S_1 = \frac{1}{\sqrt{6}} \hat{R} \left[(\sqrt{2} \delta x_{a1} + \delta z_{a1}) + (\sqrt{2} \delta y_{e1} + \delta z_{e1}) \right]$
asymmetric stretching	$e_g \epsilon$	$S_2 = \frac{1}{\sqrt{6}} \hat{R} \left[(\sqrt{2} \delta x_{a1} + \delta z_{a1}) - (\sqrt{2} \delta y_{e1} + \delta z_{e1}) \right]$
symmetric bending	$e_g \theta$	$S_3 = \frac{1}{\sqrt{6}} \hat{R} \left[(-\delta x_{a1} + \sqrt{2} \delta z_{a1}) + (-\delta y_{e1} + \sqrt{2} \delta z_{e1}) \right]$
asymmetric bending	$e_g \epsilon$	$S_4 = \frac{1}{\sqrt{6}} \hat{R} \left[(-\delta x_{a1} + \sqrt{2} \delta z_{a1}) - (-\delta y_{e1} + \sqrt{2} \delta z_{e1}) \right]$
symmetric twisting	$e_u \theta$	$S_5 = \frac{1}{\sqrt{2}} \hat{R} [-\delta y_{a1} + \delta x_{e1}]$
asymmetric twisting	$e_u \epsilon$	$S_6 = \frac{1}{\sqrt{2}} \hat{R} [\delta y_{a1} + \delta x_{e1}]$

TABLE II: Crystallographic data of some garnets: lattice constant a and special position (d) of the $Ia\bar{3}d$ (230) space group x, y, z . Local D_2 8-fold oxygen coordination of the fixed position (c) occupied by Ce as a dopant: cation-oxygen distance in the reference cube d_{ref} and D_2 displacements $S_1 - S_6$ as defined in Table I; S_1 is defined with respect to a cube with cation-oxygen distance $d = 2.34 \text{ \AA}$ (note that the use of d_{ref} , $S_1 = 0$, and $S_2 - S_6$ or $d_{ref} = 2.34 \text{ \AA}$, and $S_1 - S_6$ are two valid alternatives to define the oxygen coordinations). a , d_{ref} and $S_1 - S_6$ are given in \AA and x, y, z in fractional cell units. The lowest $4f \rightarrow 5d$ transitions calculated for the $(\text{CeO}_8)^{13-}$ clusters, embedded in a common cubic confinement potential and having the local structures of the undistorted garnets, are given in the last column in cm^{-1} ; its stabilization with respect to a reference cube of $d = 2.34 \text{ \AA}$ is given in parenthesis.

Garnet		Ref.	a	x	y	z	d_{ref}	S_1	S_2	S_3	S_4	S_5	S_6	$4f \rightarrow 5d$
Pyrope	$\text{Mg}_3\text{Al}_2\text{Si}_3\text{O}_{12}$	31	11.4566	-0.03290	0.05010	0.15280	2.243	-0.2731	-0.2191	-0.0768	-0.1215	0.9900	-0.0892	22750 (-3250)
Almandine	$\text{Fe}_3\text{Al}_2\text{Si}_3\text{O}_{12}$	32	11.5250	-0.03401	0.04901	0.15278	2.267	-0.2070	-0.2334	-0.1126	-0.1279	1.0084	-0.1028	23380 (-2620)
Spessartine	$\text{Mn}_3\text{Al}_2\text{Si}_3\text{O}_{12}$	33	11.6190	-0.03491	0.04791	0.15250	2.295	-0.1278	-0.2490	-0.1414	-0.1337	1.0281	-0.1243	24100 (-1900)
Grossular	$\text{Ca}_3\text{Al}_2\text{Si}_3\text{O}_{12}$	31	11.8515	-0.03760	0.04540	0.15130	2.368	0.0790	-0.2752	-0.2203	-0.1378	1.0725	-0.1909	25670 (-330)
LuAG	$\text{Lu}_3\text{Al}_5\text{O}_{12}$	6	11.9060	-0.02940	0.05370	0.15090	2.303	-0.1042	-0.1683	0.0555	-0.0866	0.9766	-0.1044	24910 (-1090)
YbAG	$\text{Yb}_3\text{Al}_5\text{O}_{12}$	6	11.9310	-0.02960	0.05290	0.15040	2.313	-0.0759	-0.1819	0.0497	-0.0906	0.9858	-0.1286	25140 (-860)
	$\text{Lu}_2\text{CaMg}_2\text{Si}_3\text{O}_{12}$	4	11.9750	-0.03510	0.05380	0.15780	2.333	-0.0200	-0.1522	-0.1619	-0.1139	1.0153	0.0956	25240 (-760)
ErAG	$\text{Er}_3\text{Al}_5\text{O}_{12}$	34	11.9928	-0.03039	0.05124	0.14915	2.339	-0.0039	-0.2047	0.0297	-0.0944	1.0046	-0.1854	25710 (-290)
YAG	$\text{Y}_3\text{Al}_5\text{O}_{12}$	6	12.0000	-0.03060	0.05120	0.15000	2.339	-0.0019	-0.2094	0.0156	-0.1018	1.0099	-0.1613	25680 (-320)
Andradite	$\text{Ca}_3\text{Fe}_2\text{Si}_3\text{O}_{12}$	7	12.0578	-0.03940	0.04870	0.15540	2.398	0.1648	-0.2102	-0.2895	-0.1260	1.0718	-0.0351	26210 (+210)
GdAG	$\text{Gd}_3\text{Al}_5\text{O}_{12}$	6	12.1130	-0.03110	0.05090	0.14900	2.368	0.0788	-0.2060	0.0101	-0.0932	1.0180	-0.1957	26340 (+340)
LuGG	$\text{Lu}_3\text{Ga}_5\text{O}_{12}$	6	12.1880	-0.02520	0.05700	0.15060	2.322	-0.0520	-0.1378	0.1961	-0.0727	0.9580	-0.0755	25870 (-130)
YbGG	$\text{Yb}_3\text{Ga}_5\text{O}_{12}$	6	12.2040	-0.02590	0.05630	0.15190	2.328	-0.0336	-0.1561	0.1596	-0.0899	0.9744	-0.0459	25860 (-140)
	$\text{Ca}_3\text{Sc}_2\text{Si}_3\text{O}_{12}$	7	12.2500	-0.04004	0.05010	0.15887	2.427	0.2454	-0.1972	-0.3362	-0.1401	1.0894	0.0842	26580 (+580)
YGG	$\text{Y}_3\text{Ga}_5\text{O}_{12}$	35	12.2730	-0.02740	0.05460	0.14930	2.363	0.0647	-0.1629	0.1338	-0.0757	0.9876	-0.1440	26640 (+640)
HoGG	$\text{Ho}_3\text{Ga}_5\text{O}_{12}$	36	12.2900	-0.02740	0.05520	0.15020	2.362	0.0616	-0.1550	0.1293	-0.0771	0.9861	-0.1101	26610 (+610)
DyGG	$\text{Dy}_3\text{Ga}_5\text{O}_{12}$	36	12.3060	-0.02780	0.05490	0.14990	2.369	0.0823	-0.1558	0.1194	-0.0752	0.9896	-0.1229	26740 (+740)
TbGG	$\text{Tb}_3\text{Ga}_5\text{O}_{12}$	37	12.3474	-0.02820	0.05470	0.14950	2.381	0.1166	-0.1538	0.1115	-0.0712	0.9933	-0.1377	26980 (+980)
GdGG	$\text{Gd}_3\text{Ga}_5\text{O}_{12}$	37	12.3829	-0.02890	0.05420	0.14940	2.394	0.1538	-0.1578	0.0901	-0.0719	1.0019	-0.1473	27180 (+1180)
SmGG	$\text{Sm}_3\text{Ga}_5\text{O}_{12}$	37	12.4361	-0.02920	0.05300	0.14900	2.412	0.2031	-0.1816	0.0777	-0.0818	1.0190	-0.1748	27410 (+1410)

Figure captions

FIG. 1: D_2 totally symmetric displacements of the CeO_8 moiety: Stretching, bending, and twisting O_h symmetry coordinates S_1 (a_{1g} symmetric stretching -breathing-), S_2 ($e_g\epsilon$ asymmetric stretching), S_3 ($e_g\theta$ symmetric bending), S_4 ($e_g\epsilon$ asymmetric bending), S_5 ($e_u\theta$ symmetric twisting), and S_6 ($e_u\epsilon$ asymmetric twisting). See Table I for the detailed definitions.

FIG. 2: $4f$ (dashed lines) and $5d$ (full lines) energy levels of the $(\text{CeO}_8)^{13-}$ embedded cluster (relative to the ground state) as a function of the $S_1 - S_6$ D_2 oxygen displacement coordinates, calculated without spin-orbit coupling. The differences between the $5d$ and $4f$ energy centroids (dot-dashed lines) and between the ligand field stabilization energies of the $5d$ and $4f$ lowest levels (dotted lines) are also shown; the lowest $4f \rightarrow 5d$ transition equals the subtraction of these two. Experimental values of $S_1 - S_6$ of 21 pure garnets are shown as small vertical lines.

FIG. 3: $4f$ and $5d$ energy levels of the $(\text{CeO}_8)^{13-}$ embedded cluster as a function of $S_1 - S_6$, calculated with spin-orbit coupling. All levels are $D_2' \Gamma_5$ Kramer doublets. See Fig.2 caption.

FIG. 4: $4f$ energy levels of the $(\text{CeO}_8)^{13-}$ embedded cluster as a function of $S_1 - S_6$, calculated without spin-orbit coupling. Dotted lines: 2A levels; full lines: 2B_1 levels; dashed lines: 2B_2 and 2B_3 levels. Experimental values of $S_1 - S_6$ of 21 pure garnets are shown as small vertical lines.

FIG. 5: $4f$ energy levels of the $(\text{CeO}_8)^{13-}$ embedded cluster as a function of $S_1 - S_6$, calculated with spin-orbit coupling. All levels are $D_2' \Gamma_5$ Kramer doublets. Experimental values of $S_1 - S_6$ of 21 pure garnets are shown as small vertical lines.

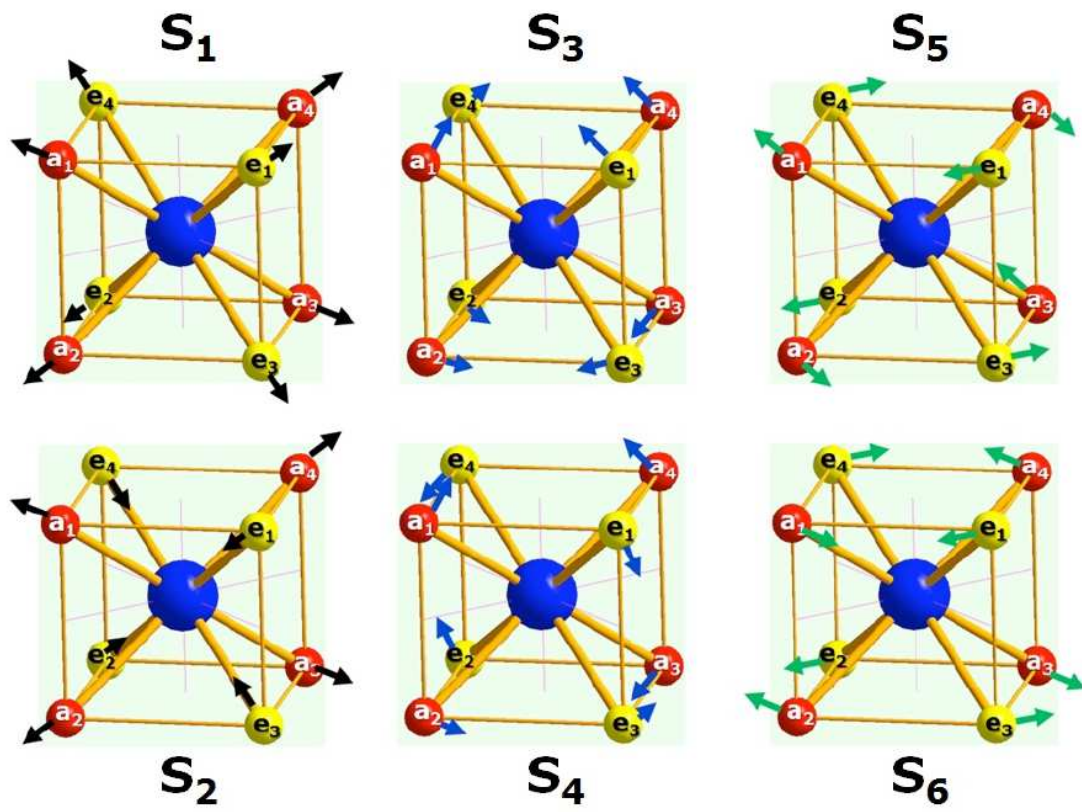


Figure 1. Seijo and Barandiarán

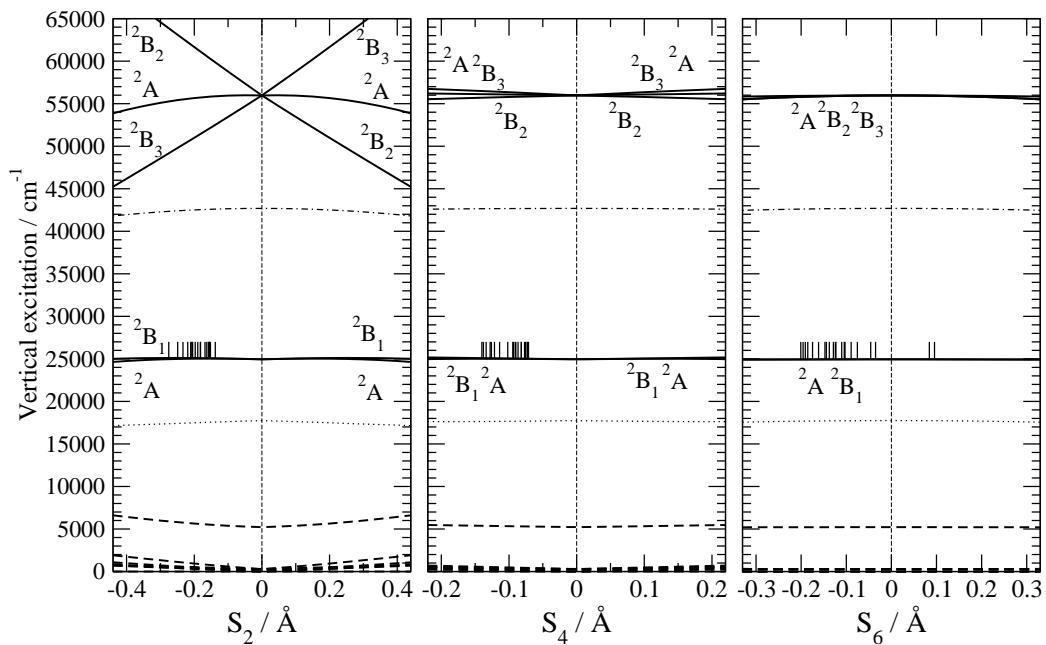
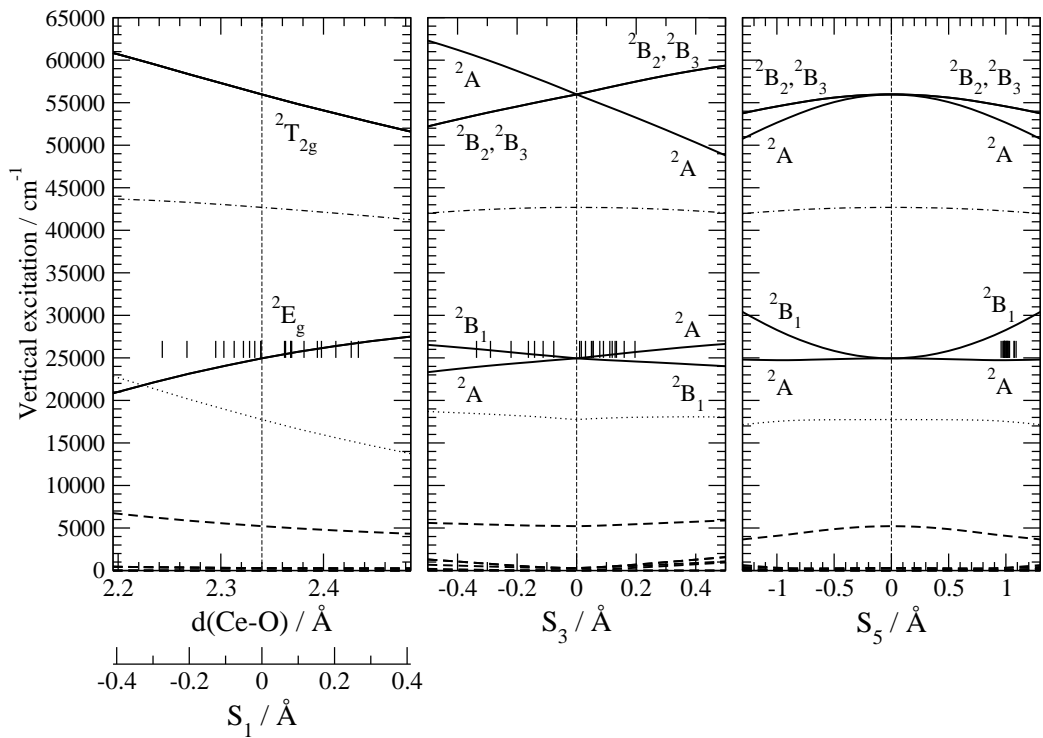


Figure 2. Seijo and Barandiarán

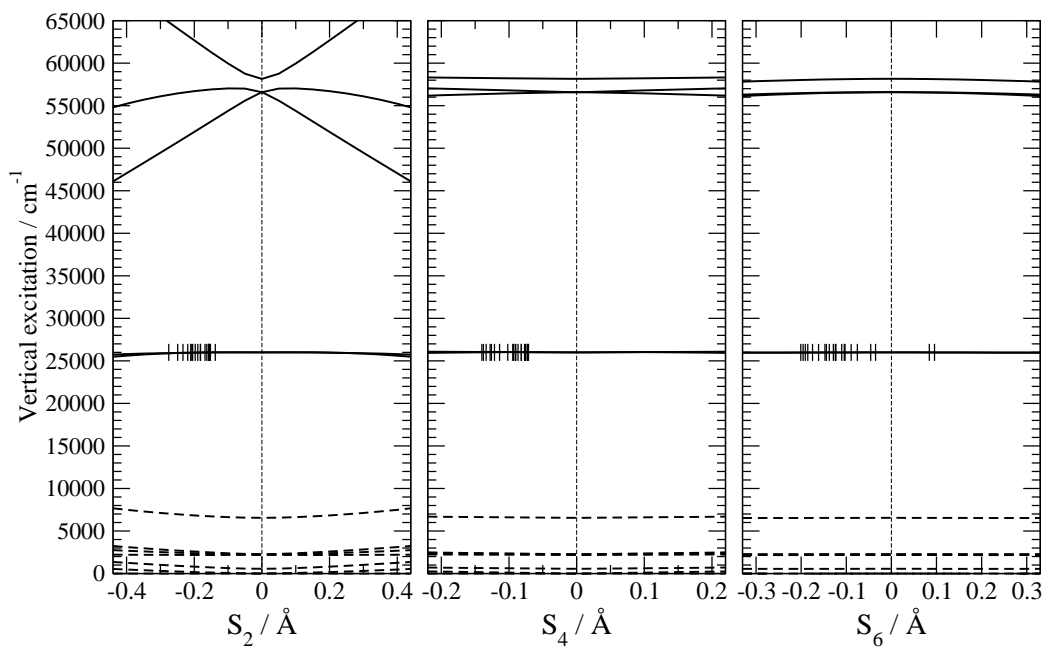
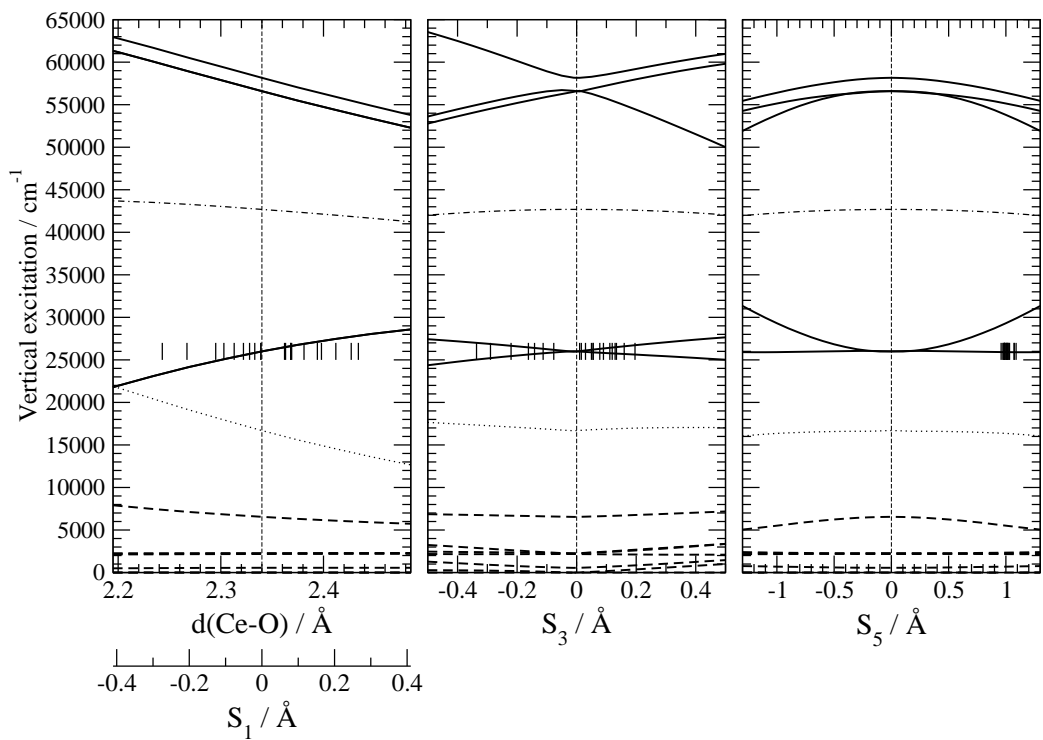


Figure 3. Seijo and Barandiarán

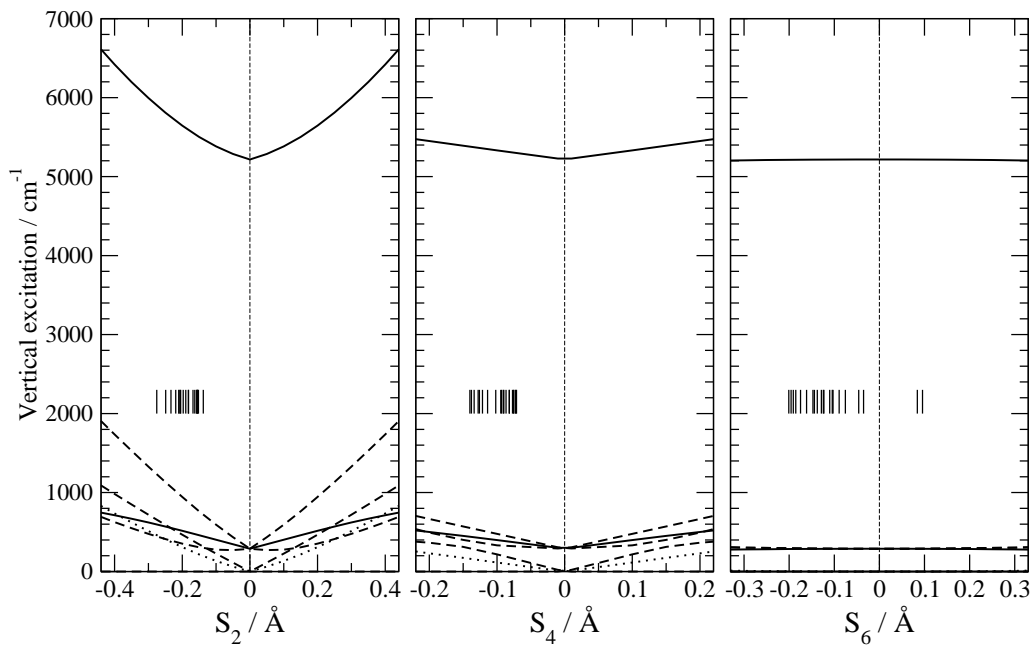
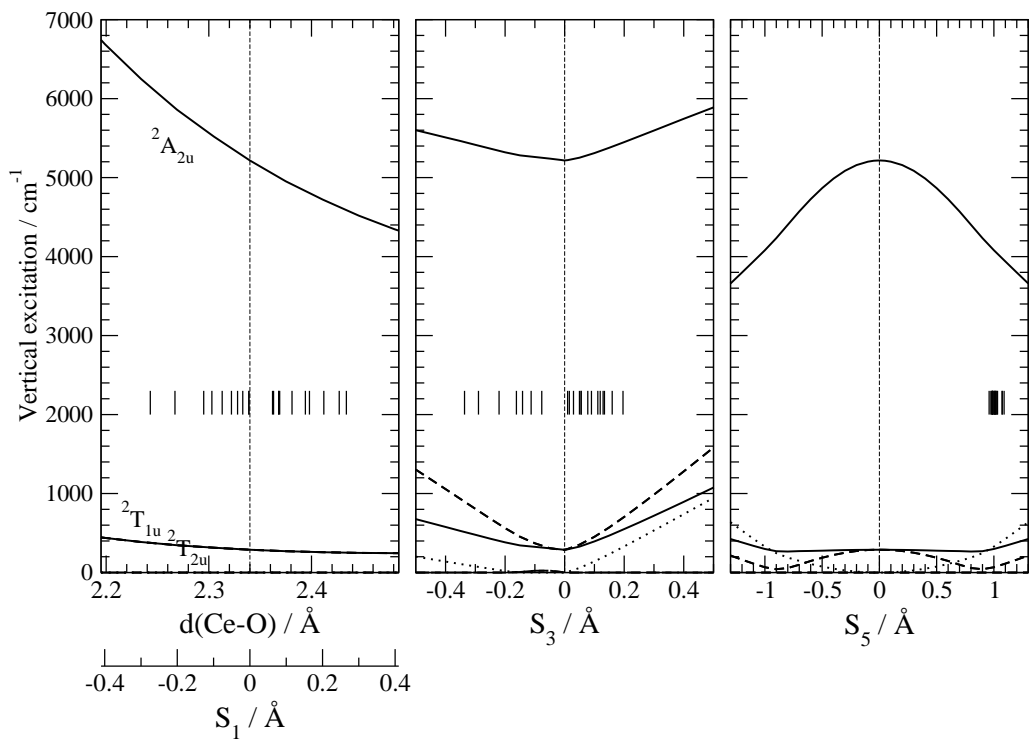


Figure 4. Seijo and Barandiarán

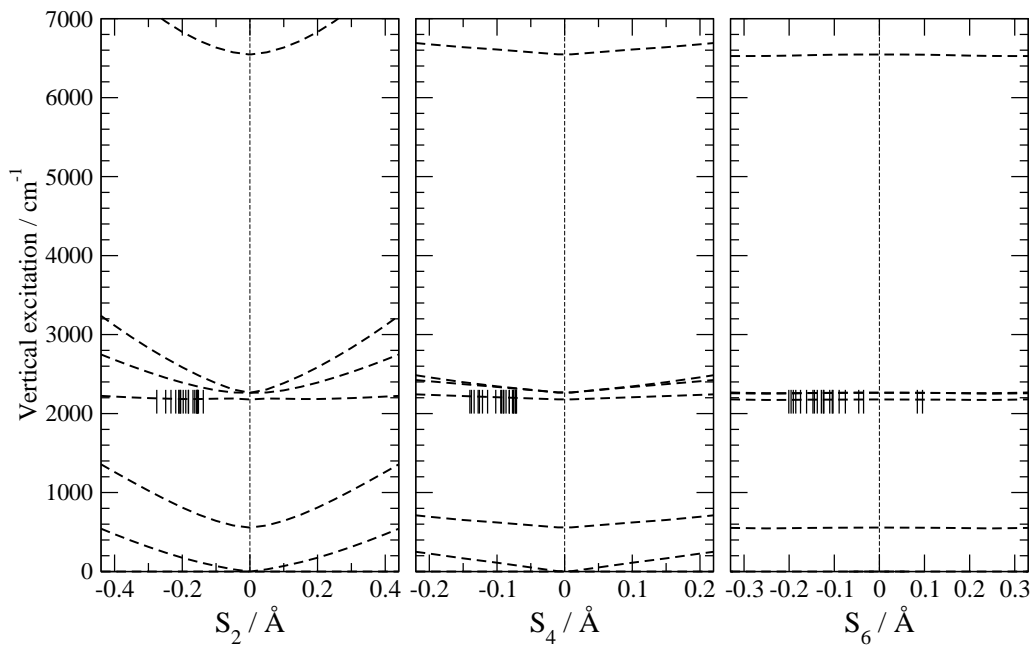
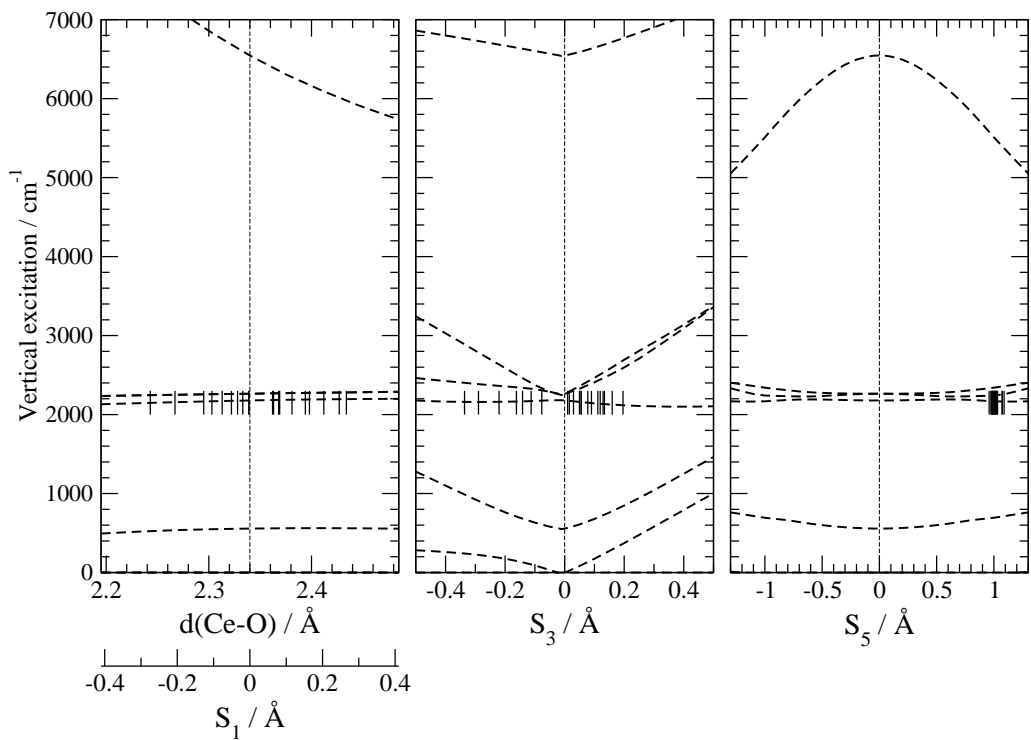


Figure 5. Seijo and Barandiarán